# Investigation and Retardation of the Dewetting on Top of Highly Viscous Amorphous Substrates

**C. Renger,[†,‡] P. Müller-Buschbaum,[*,§] M. Stamm,[⊥] and G. Hinrichsen[‡]**

*Max-Planck-Institute for Polymer Research, Ackermannweg 10, 55128 Mainz, Germany; Technical University of Berlin, Institute for Nonmetallic Materials, Polymer Physics, Englische Str. 20, 10587 Berlin, Germany; TU München, Physics Department LS E13, James-Franck-Str. 1, 85747 Garching, Germany; and Institut für Polymerforschung Dresden e.V., Hohe Strasse 6, 01069 Dresden, Germany*

*Received February 16, 2000; Revised Manuscript Received July 27, 2000*

ABSTRACT: The dewetting behavior of thin polystyrene (PS) films on top of an amorphous polyamide (PA) layer is investigated at two different annealing temperatures (119 and 195 °C). While PS is liquid at both temperatures, the PA layer remains solid at 119 °C and becomes highly viscous at 195 °C. At a constant thickness of the PA layer, the thickness and the molecular weight of the PS top layer were varied. With optical microscopy and optical phase interference microscopy ex situ the hole growth was measured during the dewetting of the PS layer. A statistical analysis of the data shows evidence for a change in the dewetting mechanism from a spinodal process into a nucleation and growth process as a function of film thickness. For very thin films the effect of a geometrical constraint is discussed. The retardation of the observed dewetting process was achieved by adding a styrene maleic anhydride random copolymer (SMA). The influence of the amount of SMA added and its molecular weight are shown for each given temperature. SMA with a low weight percentage content of maleic anhydride shows an increased retardation as compared to a higher weight percentage irrespective of the amount of SMA added.

## Introduction

Thin polymer films on top of a substrate are used in many industrial applications such as coatings, paint, adhesives, dielectrics, or optical elements.[1−3] For many applications a homogeneous polymer layer is necessary to achieve the desired properties. Different techniques exist to produce such a layer: dip-coating, floating, or spin-coating.[4] If the polymer completely *wets* the substrate, then the polymer film will remain stable with increasing temperature. The polymer layer, however, is metastable if it is deposited on top of a *nonwettable* substrate. In this case, the film may dewet the substrate when heated above its glass-transition temperature. This dewetting process is driven by long-range interactions[5] and proceeds in three characteristic steps: First, the polymer film ruptures and holes are created. Second, these holes grow with time until their rims merge and build up a network system over the whole surface. Finally, this network system decays into droplets.[6,7]

The creation of holes in the film depends strongly on the thickness of the metastable layer: Above a critical thickness $l_{c1}$ the polymer film may remain stable at all. Below $l_{c1}$, however, the film ruptures.[7] Holes are created by impurities on the substrate or in the film which is the so-called nucleation and growth process. However, below a further critical thickness $l_{c2} < l_{c1}$ another dewetting mechanism, the spinodal dewetting, becomes evident. Thermally induced surface waves lead to a breakup of the film if the amplitude of these waves reaches the total film thickness;[6,8] the theoretical aspects of dewetting have been investigated in detail elsewhere.[7,9−12] On top of a solid substrate (liquid/solid dewetting) the growth of holes depends on whether the polymer exhibits a viscous flow or slips on the substrate. In the case of a viscous flow the hole radius $R$ constantly grows with time, and the hole area $R^2$ increases by $R^2 \propto t^2$.[11] Once started by polymer slippage on the surface, the hole area increases slower with time following $R^2 \propto t^{4/3}$.[12]

When considering a liquid substrate (liquid/liquid dewetting), the substrate viscosity must be taken into account.[9] Dewetting velocity depends on the relation between the viscosity of the polymer layer $\eta_l$ and the substrate $\eta_s$. For $\eta_s > \eta_l/\theta$ ($\theta$ denoting the contact angle between film and substrate) the hole area grows according to $R^2 \propto t^2$. For $\eta_s < \eta_l/\theta$, however, the area grows by $R^2 \propto t^{4/3}$. Thus, for liquid/solid as well as for liquid/liquid dewetting, the values 2 and $^4/_3$ mark the limits of the exponent of hole growth.

Recently, the liquid/solid dewetting and liquid/liquid dewetting process has received much attention.[6,8,13−19] In the presented investigation the dewetting of polystyrene films (PS) with variable film thickness and different molecular weights on top of an amorphous polyamide layer (PA) has been determined (Figure 1). The samples were annealed at different temperatures ($T_1$ = 119 °C and $T_2$ = 195 °C). While PS is liquid at both temperatures, PA is solid at $T_1$ and becomes highly viscous at $T_2$. Thus, the rarely investigated viscosity regime between a solid and a liquidlike behavior is concentrated upon. Additionally, the retardation of the dewetting velocity by adding a copolymer, which promotes the interaction at the polymer/polymer interface, is discussed.

## Experimental Section

**Sample Preparation.** Native oxide covered silicon wafers Si (100) (MEMC Electronic Materials Inc., Spartanburg) were

[†] Max-Planck-Institute for Polymer Research.
[‡] Technical University of Berlin.
[§] TU München.
[⊥] Institut für Polymerforschung Dresden e.V.

10.1021/ma000287k CCC: $19.00 
Published on Web 10/14/2000

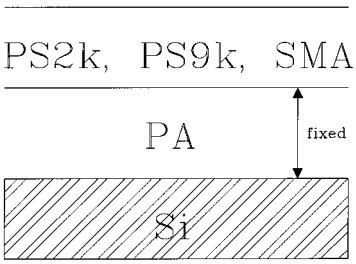


**Figure 1.** Schematic sample setup: A silicon wafer was used as substrate for the polyamide (PA) layer which was produced by a spin-coating process. This layer wetted the substrate and therefore remained stable during the entire investigation. On top of the PA layer, polystyrene (PS) films of different thickness and molecular weight were prepared using the spin-coating technique as well.

used as substrate to prepare the bilayer samples. Prior to spin-coating the substrates were cleaned. After placing them three times in dichloromethane in an ultrasonic bath for 5 min, the substrates were rinsed with Milli-Q water. (Milli-Q water is highly purified water. Typical values for this water are as follows: resistivity at 25 °C, 18.2 Mohm cm; TOC level, 5−10 ppb; particles (0.22 $\mu$m), <1/mL; microorganisms, <1 cfu/mL.) Next, they were put into an oxidation bath which consisted of 1400 mL of Milli-Q water, 120 mL of $H_2O_2$, and 120 mL of $NH_3$. The mixture was heated to 75 °C, and the substrates were kept in the solution for at least 2 h. Finally, the wafers were stored in fresh Milli-Q water until the spin-coating process was started. Immediately before coating, the substrates were dried using compressed nitrogen.

For the polymer basis layer an amorphous polyamide-6I, a condensate of isophathalic acid and diaminohexane (PA, trade name: Durethan T40 of Bayer AG, Leverkusen), with a molecular weight $M_w = 28\,900$ g/mol and a polydispersity of $M_w/M_n = 3.28$, was used.[20−23] A 310 mg sample of this polymer was dissolved in 20 mL of 1,2-chlorophenol and stirred for at least 48 h. The solution was shielded against light to avoid solvent aging. The spin-coating of this solution (2 min at 1950 rpm) yielded a homogeneous PA layer, the thickness of which was determined by X-ray reflectivity measurements.

On top of this amorphous layer polystyrene (PS) films were spin-coated (30 s at 1950 rpm) from a toluene solution. Two different molecular weights of PS, $M_w = 2160$ g/mol ($M_w/M_n = 1.04$) as well as $M_w = 8690$ g/mol ($M_w/M_n = 1.12$), were used (denoted by PS2k and PS9k). A variation of the solution concentration allowed the preparation of different film thickness.[24]

To investigate the influence of added copolymers, PS2k was blended with styrene maleic anhydride random copolymer (SMA) in solution. The SMA was used with two different weight percentage compositions of maleic anhydride, namely 2 wt % (SMA2) and 33 wt % (SMA33).[20−23] Samples containing 1, 3, 5, 10, and 30 wt % of SMA2 or SMA33 were prepared from a tetrahydrofuran solution by spin-coating (30 s at 1950 rpm). By varying the solvent concentration, a constant film thickness of all blended samples was ensured. All used polymers are listed in Table 1.

Immediately after preparation all samples were investigated using X-ray reflectivity to determine the film thickness of each homogeneous polymer layer. The samples were annealed successively on a logarithmical time scale in a vacuum furnace and quenched down to room temperature prior to investigation. Two different annealing temperatures, 119 and 195 °C, were chosen. At both temperatures PS is a liquid. PA is a solid at 119 °C and highly viscous ($\eta = 1.8 \times 10^6$ Pa s) at 195 °C.

**Optical Microscopy.** The sample surfaces were analyzed using a Zeiss Axiotech 25H optical microscope with magnifications between 4 and 50 times. A Hitachi KP-D50 CCD camera recorded the optical micrographs. The statistical analysis of each individual picture was performed with a graphics analysis program (IMAGE PRO PLUS, Silverspring, USA). This program detects characteristic features in micrographs by analyzing the gray scale distribution of the pixel in the picture. Thus, the size of all holes in each picture was detected in one step, and an average hole diameter and its standard derivation were calculated. The analysis procedure used in this investigation included a further step: In this second step the pictures were 2D Fourier transformed (fast Fourier transformation, FFT), and a most prominent in-plane length scale was extracted after a radial averaging of the resulting power spectrum density (PSD) function from these data.

**Table 1. Polymers Used in the Present Investigation[a]**

| polymer | $M_w$ [g/mol] | $M_n$ [g/mol] | $M_w/M_n$ | $N$ | $T_g$ [°C] |
|---|---|---|---|---|---|
| PA 6I | 28900 | 8800 | 3.28 | 117 | 130 |
| PS 2k | 2160 | 1970 | 1.04 | 21 | 65.7 |
| PS 9k | 8690 | 7720 | 1.12 | 83 | 92.1 |
| SMA 2 | 170000 | 100000 | 1.7 | 1587 | 109 |
| | $n$ (MA): 32 | $n$(styrene): 1555 | | | |
| SMA 33[b] | 22000 | 5000 | 4.4 | 144 | 167 |
| | $n$(MA): 47 | $n$(styrene): 97 | | | |

[a] $M_w$ and $M_n$ denote the molecular weights of the polymers as determined by GPC, $M_w/M_n$ is the polydispersity, $N$ is the degree of polymerization, and $T_g$ is the glass transition temperature as determined by DSC. [b] Number after SMA denotes weight percent of MA in SMA.

**Table 2. Overview of the Investigated Polymer Sample Series with Used Abbreviations[a]**

| sample | thickness [nm] | sample | thickness [nm] |
|---|---|---|---|
| | Polystyrene Films | | |
| PS2k-20 | 20 ± 1 | PS9k-15 | 15 ± 1 |
| PS2k-45 | 45 ± 1 | PS9k-35 | 35 ± 1 |
| PS2k-92 | 92 ± 1 | PS9k-68 | 68 ± 1 |
| PS2k-174 | 174 ± 1 | PS9k-174 | 174 ± 1 |
| PS2k-395 | 395 ± 1 | PS9k-395 | 395 ± 1 |
| | SMA Samples | | |
| SMA-0% | 13 ± 1 | SMA | 13 ± 1 |
| SMA2-1% | 13 ± 1 | SMA33-1% | 13 ± 1 |
| SMA2-3% | 13 ± 1 | SMA33-3% | 13 ± 1 |
| SMA2-5% | 13 ± 1 | SMA33-5% | 13 ± 1 |
| SMA2-10% | 13 ± 1 | SMA33-10% | 13 ± 1 |
| SMA2-30% | 13 ± 1 | SMA33-30% | 13 ± 1 |

[a] For the PS2k and PS9k series, five samples of different thickness were prepared. In both SMA series, SMA2 and SMA33, the copolymer was added to PS2k with five different weight percentages. The sample SMA-0% is a pure PS2k sample with no SMA added. In the text, abbreviations such as PS2k-20, PS9k-15 (where the last number stands for the film thickness), and SMA2-1% (where the last number stands for the SMA*x* content) are used.

**Phase Measuring Interference Microscope.** For further optical characterization of the samples a LOT/Zygo phase measuring interference microscope with a lateral resolution of approximately 1 $\mu$m and a height resolution better than 1 nm was used. The interference pattern of monochromatic light reflected from a flat reference surface and from the investigated sample was recorded in an area detector while the reference plane is moved with a piezoelectric device.[25] A magnification of 10 and 100 times, respectively, was used. The data analysis was performed from an area of 50.40 $\mu$m × 46.60 $\mu$m and 499.60 $\mu$m × 461.80 $\mu$m.

**X-ray Reflectometry.** Reflectivity curves were measured using a 12 kW rotating anode with a copper target and a graphite monochromator crystal (wavelength 0.154 nm). The film thicknesses of all samples were determined right after preparation. Irrespective of the type of sample investigated, all reflectivity curves showed well-pronounced fringes resulting from a small interface and surface roughness. This confirmed the presence of homogeneous polymer layers. The thickness of the PA sublayer was determined to be 46 ± 1 nm for all PS2k and PS9k samples and 43 ± 1 nm for the SMA samples. The top layer thickness was varied between 13 ± 1 and 395 ±

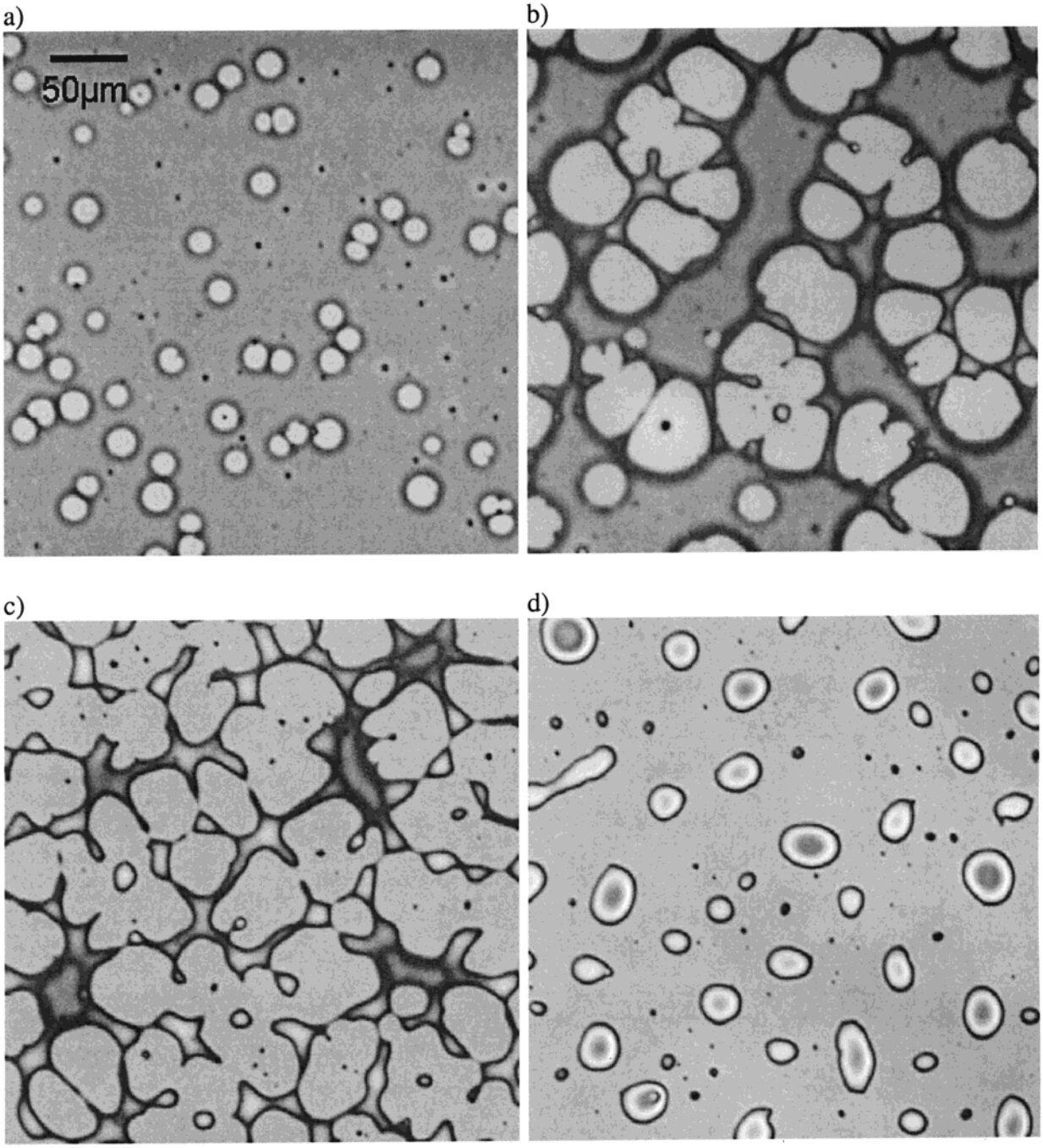


**Figure 2.** Sample PS2k-20 after (a) 19.67, (b) 107.67, (c) 147.67, and (d) 1076.17 h annealing in a vacuum furnace at 119 °C. Note that the holes in parts a and b seem to have almost identical diameters.

2 nm. Table 2 includes the measured values and introduces the used abbreviations (e.g., PS2k-20, PS9k-35, or SMA2-1%).

## Results and Discussion

**Liquid/Solid Dewetting.** In the investigated molecular weight range PS at 119 °C is a fluid whereas the PA sublayer can be regarded as a solid. The evolving surface morphologies depended strongly on the molecular weight of the PS layer. The PS9k samples were stable irrespective of the film thickness. Even after 1860 h the surface remained homogeneous without any holes. Contrary, the PS2k samples dewetted the PA layer. As an example, data from the sample of the smallest film thickness, PS2k-20, are presented. Figure 2 shows optical micrographs taken of sample PS2k-20 after four different annealing times. These times were chosen to present typical morphologies. After 19.67 h annealing at 119 °C (Figure 2a) holes of an approximately equal size had been developed. Black spots are visible inside some holes, indicating that a nucleation and growth process was the leading dewetting mechanism, although the similar size of holes is unusual for such a process. A possible explanation might be given by the small thickness of the PS films, which enables heterogeneous nucleation. Large as well as very small particles acted as nucleation sites. Thus, most holes were created at the same time and, as a consequence, had a similar size. The diameter of these holes increased with time, and after 107.67 h (Figure 2b) some holes had combined with others. At that time, rims started to build up a regular network over the whole sample area. Further annealing led to a breakup of this network into drops (Figure 2c).

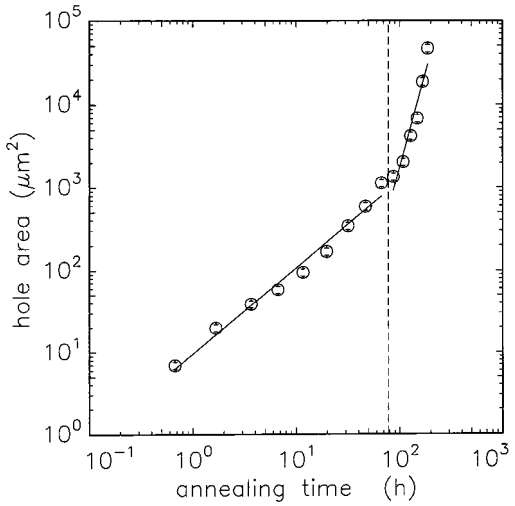


**Figure 3.** Average area of holes of sample PS2k-20 as a function of annealing time. The dashed line denotes the time when the holes merge. The solid lines show fits resulting from a linear regression analysis. For the time before the holes merge, a slope of $n = 1.05 \pm 0.05$ is observed while this value is much higher after the holes have been combined ($n = 4.5 \pm 0.6$).

Later, isolated, single drops evolved (Figure 2d). The drop diameter depended on the originally prepared film thickness.

The average hole area as a function of annealing time is presented in Figure 3. The dashed line denotes the time at which the holes began to combine. For longer annealing times the holes coalesced, and thus the graphics image analyzing program was not able to detect the individual holes any more. Instead, the program interpreted the combined area of several holes as one big hole, and thus the average area of all holes seemed to grow much faster. Applying a linear regression analysis to the data, the initial slope was determined to be $1.05 \pm 0.05$ whereas, after the holes have merged, the slope increased to $4.5 \pm 0.6$ (Figure 3). With increasing thickness of the PS films (samples PS2k-45, -92, -174, and -395) the dewetting process was retarded. However, as discussed later, this retardation was not due to a change of the hole growth exponent but due to a lower number of holes occurring in thicker films. We found for the complete investigated range of PS2k film thicknesses that the time dependence of the average hole area growth is similar.

As described in the Experimental Section, the optical micrographs were Fourier transformed and the power spectrum density function was determined. As an example, Figure 4a presents the radial averaged power spectrum density function of sample PS2k-20 exhibiting two maxima at $q_{m1}$ and $q_{m2}$. $q_{m1}$ corresponds to the diameter of the holes in the PS film, whereas $q_{m2}$ seems to be the second-order peak of $q_{m1}$. Obviously, the hole size distribution remained quite monodisperse during the dewetting process, which is shown in real space in Figure 2. For the samples PS2k-20, -45, and -92 two maxima (most prominent wave vector value) $q_{m1}$ and $q_{m2}$ were determined, while for PS2k-174 and -395 no maxima were observable. This might result from the limited number of holes inside the area of the optical micrograph.

In Figure 4b the dominant wave vector values of $q_{m1}$ (open circles) and $q_{m2}$ (filled circles) are plotted as a function of annealing time. As expected, both values

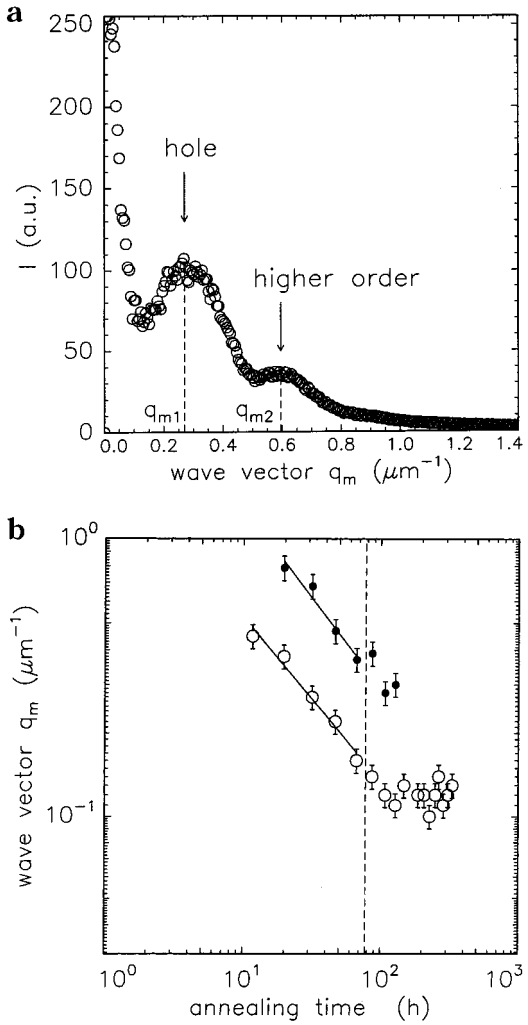


**Figure 4.** (a) Radially averaged power spectrum density function of sample PS2k-20 after 31.67 h annealing at 119 °C. Two maxima can be detected: $q_{m1}$ and $q_{m2}$. Calculating the wavelength $\Lambda = 2\pi/q_m$ shows that $q_{m1}$ corresponds to the average hole diameter at this time of the dewetting process. $q_{m2}$ denotes a higher order of $q_{m1}$ only and therefore also describes the average hole diameter. The existence of a higher order value indicates that the hole size distribution was very narrow, and almost all holes had a similar diameter. (b) Most prominent in-plane wave vector as a function of annealing time (sample PS2k-20). The dashed line denotes the time when the holes are combined. The open circles describe the $q_{m1}$ values and the filled circles $q_{m2}$. As expected, since $q_{m2}$ is a higher order of $q_{m1}$ only, both wave vectors decrease with annealing time. After the holes have merged, the $q_{m1}$ value becomes constant at $q_{m1} = 10^{-1}\ \mu$m$^{-1}$. Calculating $\Lambda = 2\pi/q_m$ gives $\Lambda = 50\ \mu$m, which fits to the distance of the polystyrene material on the surface after the holes have merged (Figure 2c).

decrease for short annealing times. The most prominent in plane length ($\Lambda = 2\pi/q_{m1}$) here corresponds to the hole diameter. The dashed line again denotes the time when holes had merged. For shorter times a slope of $n = -0.6 \pm 0.1$ was determined. Since most of the holes in sample PS2k-20 were of a similar size, they combined at the same time, and thus their growth was rapidly depressed. This is shown in Figure 4b; after ≈150 h annealing, the wave vector values reached a constant value of $q_{m1} \approx 10^{-1}\ \mu$m$^{-1}$. The corresponding value of $\Lambda = 2\pi/q_{m1} \approx 50\ \mu$m fits very well to the distance of the rims after the holes have been combined (Figure 2c). Thus, for long annealing times, this different feature is detected as a most prominent in-plane length from the FFT.

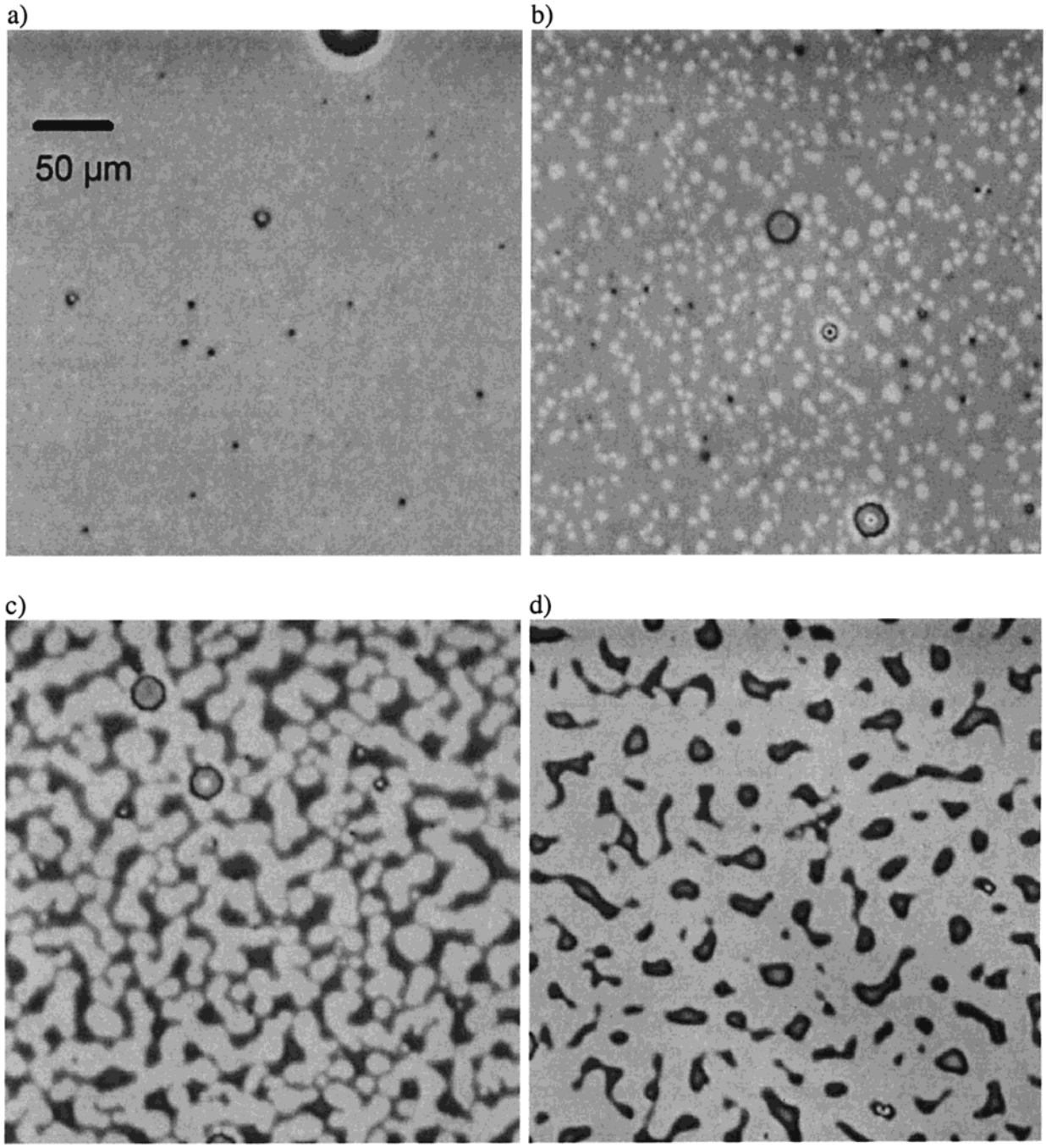


**Figure 5.** Sample PS9k-15 after (a) 42, (b) 86.5, (c) 125.5, and (d) 274 h annealing in a vacuum furnace at 195 °C. Note that the number of holes created (patrs a and b) is different from that of sample PS2k-20 (Figure 2). In sample PS9k-15 holes occur almost everywhere on the surface, whereas the number of holes in sample PS2k is much lower.

**Liquid/Highly Viscous Liquid Dewetting.** At the second annealing temperature ($T$ = 195 °C) PS again is liquid for the investigated molecular weight range, whereas the PA sublayer changes its character: The viscosity of PA ($\eta_{PA} = 1.8 \times 10^6$ Pa s) at 195 °C is still high compared to the viscosity of PS9k ($\eta_{PS9k} = 1.55$ Pa s) (compare viscosity of glycerine at room temperature: 1.53 Pa s), but it is not longer a solid which yields deviations from the common liquid/solid dewetting. Additionally, changing the annealing temperature effects also the mobility of the polymer molecules. Following the temperature−time equivalence, e.g., expressed by the WLF equation, 1 h at 195 °C is equivalent to 66 600 h at 119 °C. Thus, the chosen annealing temperature was expected to influence the dewetting velocity observed in the experiments. Indeed, we detected an accelerated dewetting of the PS2k samples. Moreover, the PS9k samples, which remained stable at 119 °C, now also dewetted the substrate, thereby exhibiting a different type of dewetting.

As an example of this the data from the sample with the smallest film thickness are presented: Figure 5 shows optical micrographs of the sample PS9k-15. After 42 h (Figure 5a) the PS film was still homogeneous, and no indication of a dewetting was detected. However, after 86.5 h uniform holes occurred over the whole sample again (Figure 5b). In contrast to the PS2k samples annealed at $T$ = 119 °C, we did not observe any particles inside these holes which might be taken as a first indication of an absence of a nucleation

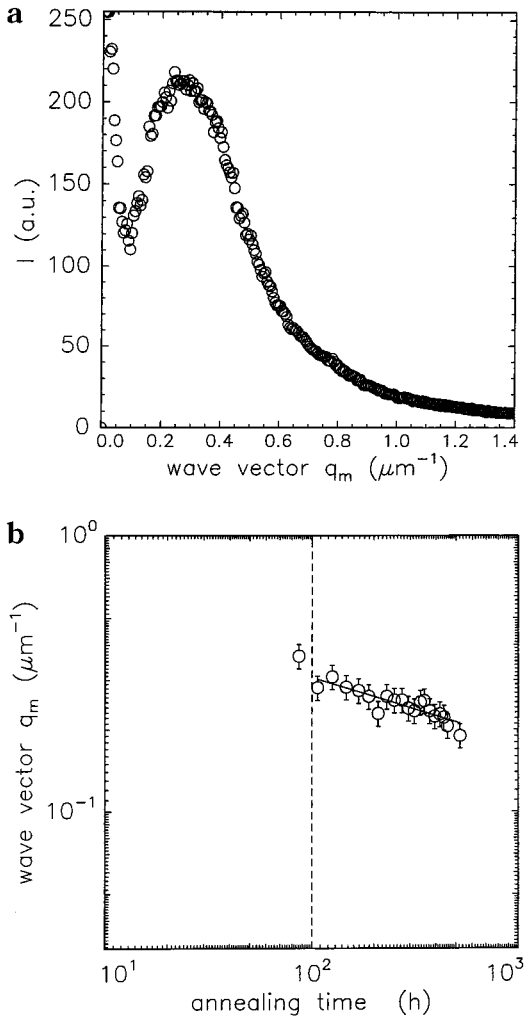


**Figure 6.** (a) Power spectrum density of sample PS9k-15 after 146.5 h annealing at 195 °C. One maximum is detected which corresponds to a most prominent in-plane wave vector value. (b) Most prominent in-plane wave vector as a function of annealing time (sample PS9k-15). The dashed line denotes the time when holes merge. The solid line shows a fit resulting from a linear regression analysis with a slope of $n = -0.22 \pm 0.02$.

process. With further annealing the holes grew and merged. Thus, a network of the rims of the holes was generated (Figure 5c). During the following annealing steps this network broke up, and finally PS drops were formed (Figure 5d). A similar behavior of the dewetting process was observed in a film with a thickness of 35 nm (PS9k-35). Both similar dewetting patterns correspond to a spinodal pattern reported by Sung et al.,[26] and thus the conclusion might be drawn that these samples dewetted via a spinodal process rather than a nucleation process. Figure 6a presents the PSD spectrum of sample PS9k-15 after a Fourier transformation of the optical micrographs. In contrast to Figure 4a, only one intensity maximum located at a most prominent wave vector value $q_m$ is present. The calculated most prominent in plane length $\Lambda = 2\pi/q_m$ again corresponds to the average hole diameter. In Figure 6b the maximum wave vector value as a function of annealing time is presented. From a linear regression analysis a slope of $-0.29 \pm 0.06$ was determined. The slopes of all samples obtained from the PSD analysis are listed in Table 3. The time interval during which individual holes grew independently is denoted with slope I. After holes

**Table 3. Slope of the Wave Vector Value $q_m$ at the Beginning (Slope I) and at the End (Slope II) of the Dewetting Process**

| sample | slope I | slope II |
|---|---|---|
| PS2k-20 ($T = 119$ °C) | $-0.59 \pm 0.05$ | $0.0 \pm 0.1$ |
| PS2k-45 ($T = 119$ °C) | $-0.48 \pm 0.02$ | $-0.68 \pm 0.25$ |
| PS2k-92 ($T = 119$ °C) | $-0.28 \pm 0.01$ | |
| PS9k-15 ($T = 195$ °C) | $-0.29 \pm 0.06$ | $-0.49 \pm 0.09$ |

have merged, a changed time dependence is observed (slope II). Following Hashimoto et al.,[27] $\Lambda = 2\pi/q_m$ is the wavelength of the dominant mode of composition variation during a spinodal decomposition process. As a function of annealing time, the slope of the $q_m$ data should increase from $-1/3$ in the beginning to $-1$ in the end. Since the theory of spinodal dewetting is derived from the theory of decomposition, $q_m$ should follow a $t^n$ power law.[7] Note that, for short annealing times in our dewetting investigations, $q_m$ describes the diameter of the holes and not the distance between the holes on the surface. However, when the holes were combined with each other and the rims built a network over the sample surface, the size of the holes is equivalent to the distribution of the "PS phase". At this time the $q_m$ vector (slope 2 in Table 3) is expected to satisfy the theory. Sung et al.[26] determined $n_1 = -0.44 \pm 0.02$ and $n_2 = 0$ for the decomposition of a PSD/PB sample. Xie et al.[13] obtained $-0.43 \pm 0.01$ for the late stage of the spinodal dewetting process. This value agrees very well with the values of PS9k-15 and confirms the assumption that this sample dewetted via a spinodal process.

With an increase of the PS9k layer thickness, the dewetting behavior changed its character to a nucleation and growth process: Samples PS9k-174 and PS9k-395 did not show any regular pattern during dewetting. All holes had different diameters and black spots were present in their centers. This observation is taken as evidence for a crossover from spinodal to nucleated dewetting. We detected the beginning and the end of this crossover process which suggests that it covers a certain film thickness range: Figure 7 exhibits a dewetting pattern of sample PS9k-35 after 42 h (Figure 7a) and one of sample PS9k-68 after 182 h (Figure 7b). Although PS9k-35 basically seemed to dewet via a spinodal process, the analysis of Figure 7a suggests that there were also some holes generated via a nucleation process. However, as mentioned above, the FFT analysis confirmed that the spinodal process was the predominant one. Obviously this tendency to nucleation was intensified with increasing PS layer thickness. Figure 7b still shows a regular pattern in the dewetting process of PS9k-68, but many holes now had impurities located in their centers and these holes disturbed the regularity of the dewetting pattern. This suggests that the crossover started at a film thickness of $\approx$35 nm and was almost completed at a film thickness of $\approx$68 nm.

Such a crossover between the two competing processes—impurity induced nucleation and growth and spinodal dewetting due to thermally amplified surface waves—is possible due to differences in the characteristic time constants of the two processes. At a small film thickness $l$ surface waves are quickly leading to a film rupture. At a large film thickness the effect of impurities becomes dominant because the typical time constant of the spinodal dewetting grows with increasing film thickness according to $\tau \propto l^5$. A similar effect was reported by Segalman et al.[15] for poly(styrene-*co*-acrylonitrile) on PS. Xie et al.[13] also detected a crossover

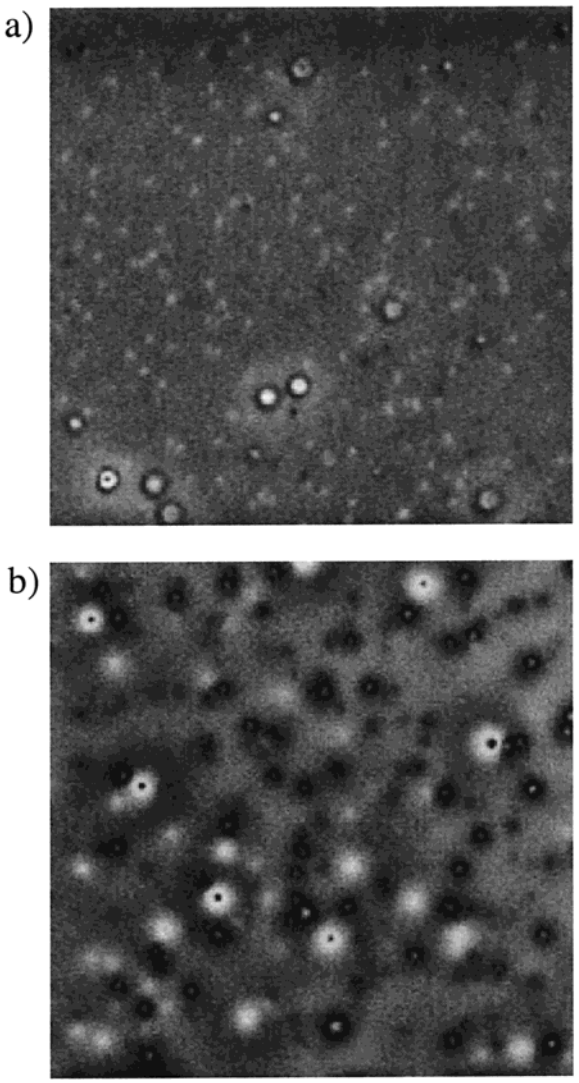


**Figure 7.** Sample PS9k-35 after 42 h (a) and sample PS9k-68 (b) after 182 h annealing at 195 °C. The two pictures show the beginning (a) and the end (b) of the crossover process from spinodal to nucleated dominated dewetting.

from spinodal to nucleated dewetting for PS films ($M_W$ = 4000 g/mol) at a thickness of 12.5 nm. From the comparison of 12.5 nm for PS4k and between 35 and 68 nm for PS9k, one might assume that the crossover thickness is molecular weight dependent. Our observations on the PS2k samples would fit this assumption. The PS2k samples showed no spinodal dewetting phenomena. All samples (including SMA-0%, which was a pure PS2k sample) dewetted by a nucleation and growth process. Assuming a molecular weight dependency of the crossover thickness, for low molecular weight polystyrene like PS2k a crossover to spinodal dewetting may be found at a film thickness well below 12 nm. In this film thickness regime, investigations require techniques with enhanced resolution such as atomic force microscopy due to the very small resulting structures. In addition, time-resolved measurements are difficult due to the very fast process. In general, any molecular weight dependency seems to be surprising since viscosity effects both processes, nucleation and spinodal dewetting, in a similar way. It is emphasized that the molecular weight investigated in the reported studies[13] as well as in this one is quite low. Thus, viscoelastic effects associated with higher molecular weights could

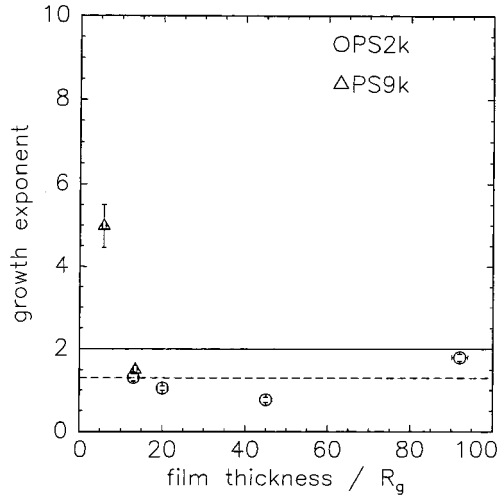


**Figure 8.** Exponent of hole growth as a function of film thickness normalized by the radius of gyration ($R_g$). The triangles denote the PS9k samples whereas the open circles are the PS2k samples. The first circle (thickness/$R_g \approx 13$) represents the SMA-0% sample, which is also pure PS2k with no SMA added. The dashed and solid lines denote the lower and upper theoretical limit of the exponent value.[7,9]

have a significant impact on the entire dewetting including a suppression of one destabilization route. It should also be noted that a differently chosen annealing temperature might shift the crossover film thickness as well. The change of the glass-transition temperature $T_g$ of thin polymer films with decreasing film thickness is a frequently investigated topic. For PS films on top of solid substrates a decrease of ~10K was reported[28] for a very similar molecular weight and film thickness range. In the case of free-standing films this decrease is even more drastic.[29] Although a highly viscous substrate is neither solid nor absent anyhow, a decrease of the glass-transition temperature for thin films seems to be reasonable.

The increase of the average hole area as a function of annealing time was also investigated for the PS9k samples, indicating the type of polymer movement during the dewetting (hole growth regime). In Figure 8 the exponent of the hole growth of all samples is plotted as a function of film thickness normalized by the radius of gyration $R_g$ of the unperturbed molecule. Triangles denote the PS9k samples, and circles denote the PS2k samples. All samples with a film thickness normalized by $R_g$ which is larger than 10 show growth exponents well below 2.0. At 195 °C it is $\eta_{PA} > \eta_{PS9k}/\theta = 29.8$ Pa s with the experimentally determined contact angle $\theta = 3°$ of PS9k on PA. Thus, even in the highly viscous regime a liquid/liquid dewetting behavior should be theoretically neglected. This indicates that a solidlike slippage of the PS films occurred according to theory irrespective of the viscosity of the underlying polymer layer[12] within the investigated range. However, for the sample PS9k-15 (film thickness/$R_g \approx 5$) a much higher growth exponent of approximately 5 was observed. Such a high value cannot be explained by conventional hydrodynamic models.[9] Since the PS film of this sample was very thin, a combination of three-dimensional and two-dimensional processes might be the reason for this outstanding value.[30,31] Recently, in the literature a different dewetting behavior for confined films compared to thin films has been reported.[32,33] Further, no marked film thickness dependence of the growth exponent of the PS2k samples was detectable. Thus, the retardation of

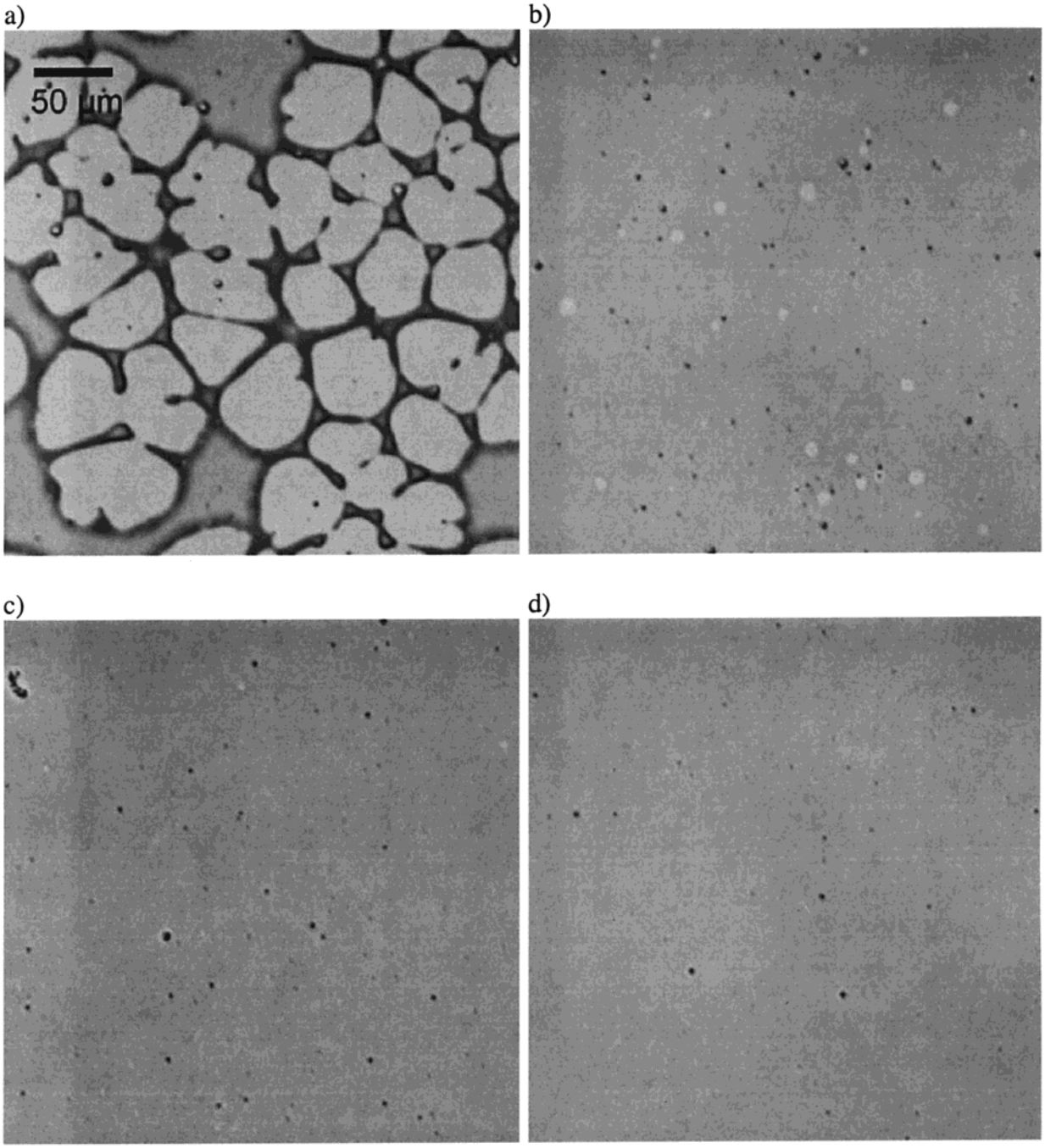


**Figure 9.** Sample SMA2: PS2k blended with SMA at different levels: (a) 0 wt % SMA2, (b) 1 wt % SMA2, (c) 3 wt % SMA2, and (d) 5 wt % SMA2 after 130.5 h annealing in a vacuum furnace at 119 °C. Note that only parts a and b show dewetting effects. In parts c and d the PS/SMA films remained unaltered, which shows a very effective retardation of dewetting.

the dewetting process determined with increasing film thickness (e.g., PS2k) was due to a lower number of holes developing in thicker films, not due to a slower hole growth. However, the growth exponents of PS2k-20 and PS2k-45 were determined to be below the lower theoretical limit of $^4/_3$. These values are unexpectedly low, and further investigations are required here.

**Retardation of Dewetting.** To influence and retard the dewetting velocity of PS on PA, PS2k was blended with SMA2 and SMA33, respectively (see Table 2). In Figure 9 the optical micrographs of the sample blended with 0 (a), 1 (b), 3 (c), and 5 wt % (d) SMA2 are shown after 130.5 h of annealing at 119 °C. It can be clearly seen that the dewetting process was retarded very effectively. Without adding SMA (Figure 9a), large holes of approximately 50 $\mu$m diameter occurred after this annealing time. Some of them already merged with their neighbors. However, with 1 wt % SMA2 added to PS2k (Figure 9b), the holes grew much slower, and thus an average diameter of 10 $\mu$m only was observed after 130.5 h annealing. In addition, the number of holes created in the film was decreased. For higher blending levels of SMA2 in PS2k this trend was enhanced: After 130.5 h annealing the samples with 5 wt % or more (10, 30 wt %) SMA2 added (Figure 9d) showed no dewetting characteristics at all.

In Figure 10 the micrographs of SMA33 samples are plotted. These samples were also annealed for 130.5 h at 119 °C. Compared to the SMA2 series the retardation was weaker. With 1 wt % SMA33 added to PS2k (Figure

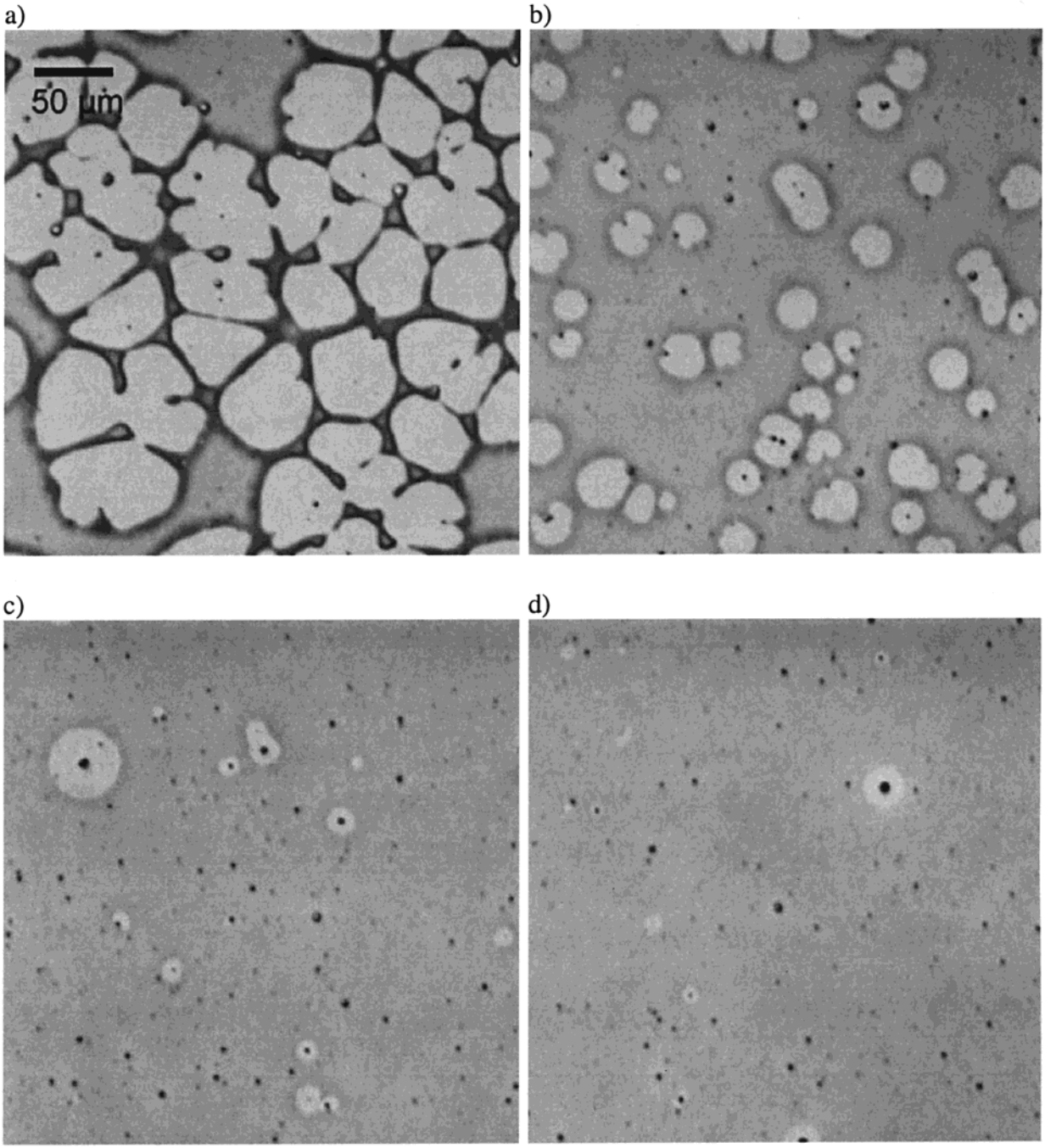


**Figure 10.** Sample SMA33: PS2k blended with SMA at different levels: (a) 0 wt % SMA33, (b) 1 wt % SMA33, (c) 3 wt % SMA33, and (d) 5 wt % SMA33 after 130.5 h annealing in a vacuum furnace at 119 °C. Note that parts c and d show some dewetting effects, whereas the equivalent samples of the SMA2 series did not. With SMA33 the dewetting is retarded but not as strong as in sample SMA2.

10b) the number of holes, which developed, was not reduced compared to the pure PS2k sample (Figure 10a). However, the holes were much smaller ($\approx 20\ \mu$m), indicating that the dewetting velocity was reduced. The influence of SMA33 on the exponent of hole growth is shown in Figure 11. The slope was reduced by 50% from $n = 1.31 \pm 0.09$ (0 wt % SMA33) to $n = 0.69 \pm 0.07$ (1 wt % SMA33). With higher blending levels of SMA33 the retardation increases: At 5 wt % SMA33 holes with big nuclei in the center (Figure 9d) were detected. At 10 wt % as well as 30 wt % SMA33 no dewetting phenomena were observed at all. From the presence of particles inside the holes we conclude a nucleation and growth mechanism for the dewetting process.

Taking into account the amount of MA groups (33 and 2 wt %) only, the higher effectiveness of SMA2 as a retarding agent might be unexpected. The MA groups build up hydrogen bonds with the PA molecules in the sublayer. Therefore, more MA groups should result in stronger bonding and thus in an enhanced retardation. A chemical reaction between SMA and amino groups leading to a graft copolymer[21,22,23] could also be possible but is very unlikely at the chosen annealing temperature. At sufficiently higher temperatures compatibility due to reaction of PS/SMA/PA blends was reported in the literature. Our results become explicable if the annealing temperature is considered with respect to the individual glass transition temperatures. The glass

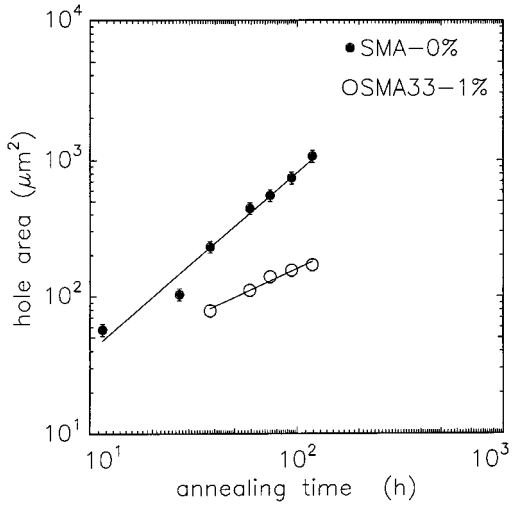


**Figure 11.** Retardation of the dewetting velocity adding 1 wt % SMA33 compared to a pure PS2k film. The filled circles show the average hole area of a pure PS2k sample (SMA0%) and the open circles SMA33-1% (1 wt % SMA33 added to PS2k). From a linear regression analysis the slopes $n = 1.31 \pm 0.09$ (SMA0%) and $n = 0.69 \pm 0.07$ (SMA33-1%) were determined.

transition temperature ($T_g$) of SMA2 is much lower ($T_g$ = 109 °C) than that of SMA33 ($T_g$ = 167 °C). Therefore, at $T$ = 119 °C SMA2 possesses a higher mobility with respect to SMA33. In addition, the PS−SMA*x* phase diagram also needs to be discussed. For SMA*x* with $x > 10\%$ the blend with PS is no longer miscible.[34] Thus, PS2k and SMA33 should yield phase separation morphologies inside the top layer. In contrast, PS2k is a good solvent for SMA2. Because of the low molecular weight of the PS, which is below the entanglement molecular weight, the SMA2 molecules can diffuse free inside the PS2k matrix. This enables a better movement to the PS/PA interface, and thus a strong bonding between the polymer layers may be achieved faster. Further, SMA2 molecules have a higher degree of polymerization ($n$ = 1587) and thus are much longer than the SMA33 molecules ($n$ = 144). This may lead to a larger number of contacts with the polymer chains at the interface and to a stronger adhesion between the layers. Such an interdiffusion of polymer chains at a polymer/polymer interface was also found by Scott et al.[35] for the system SMA/Nylon11. Cho et al.[36] observed a substantial increase of interfacial fracture toughness between $\omega$-aminopolystyrene and SMA. Thus, SMA established compatibility between amino groups (like in PA) and polystyrene, which was similarly reported by Dedecker et al.[20]

## Summary

The dewetting of PS on PA and its retardation was investigated as a function of the PS film thickness, molecular weight, and annealing temperature. In the case of PS2k annealed at 119 °C (liquid/solid dewetting), destabilization via a nucleation and growth process occurred over the whole investigated range of film thicknesses. The exponent of hole growth was independent of film thickness, and in thin films, more holes were created than in thick films, which led to a faster dewetting process. The dewetting was retarded with a high efficiency by adding copolymer SMA2 or SMA33, respectively.

In the case of PS9k films annealed at 119 °C (liquid/solid dewetting) no dewetting was observed. Those films remained stable throughout the time period of investigation. However, at 195 °C (liquid/highly viscous liquid dewetting) the samples show evidence for a dewetting via a spinodal process (film thickness less than 35 nm) and a nucleation and growth process (film thickness more than 68 nm). Thus, a crossover between spinodal and nucleation processes was obtained. A possible molecular weight dependency of this crossover process was discussed. For very thin films, the growth exponent was unexpectedly high. A possible explanation could be a combination of a three-dimensional and a two-dimensional dewetting processes.

**Acknowledgment.** We thank M. Bach for his help with the X-ray measurements. A. Best and A. Hanewald determined the viscosity values of the polymers used. Additionally, we owe many thanks to O. Wunnicke for helpful discussions and valuable assistance. We are also grateful to M. Szablewski and A. Genovese for comments on the manuscript. This work was supported by the DFG Schwerpunktprogramm "Benetzung und Strukturbildung an Grenzflächen" (Sta 324/8-1).

## References and Notes

(1) Singh, J.; Agrawal, K. K. *J. Macromol. Sci., Rev. Macromol. Chem. Phys.* **1992**, *32*, 521−534.
(2) Dautzenberg, H.; Jaeger, W.; Kötz, J.; Philipp, B.; Seidel, C.; Stscherbina, D. In *Polyelectrolytes*; Hanser Publisher: München, 1994.
(3) Roberts, J. C. In *The Chemistry of Paper*; RCS: Cambridge, 1996.
(4) Lawrence, C. J. *Phys. Fluids* **1988**, *31*, 2786−2795.
(5) Dietrich, S. In *Phase Transitions and Critical Phenomena*; Domb, C., Lebowitz, J. L., Eds.; Academic Press: New York, 1988; Vol. 12.
(6) Reiter, G. *Phys. Rev. Lett.* **1992**, *68*, 75−78.
(7) Brochard-Wyart, F.; Redon, C.; Sykes, C. *C. R. Acad. Sci., Ser. II* **1992**, 19−24.
(8) Reiter, G. *Langmuir* **1993**, *9*, 1344−1351.
(9) Brochard-Wyart, F.; Martin, P.; Redon, C. *Langmuir* **1993**, *9*, 3682−3690.
(10) Fondecave, R.; Brochard-Wyart, F. *Macromolecules* **1998**, *31*, 9305−9315.
(11) Redon, C.; Brochard-Wyart, F.; Rondelez, F. *Phys. Rev. Lett.* **1991**, *66*, 715−718.
(12) Redon, C.; Brzoska J. B.; Brochard-Wyart, F. *Macromolecules* **1994**, *27*, 468−471.
(13) Xie, R.; Karim, A.; Douglas, J. F.; Han, C. C.; Weiss, R. A. *Phys. Rev. Lett.* **1998**, *81*, 1251−1254.
(14) Qu, S.; Clarke, C. J.; Liu, Y.; Rafailovich, M. H.; Sokolov, J.; Phelan, K. C.; Krausch, G. *Macromolecules* **1997**, *30*, 3640−3645.
(15) Segalman, R. A.; Green, P. F. *Macromolecules* **1999**, *32*, 801−807.
(16) Bischof, J.; Scherer, D.; Herminghaus, H.; Leiderer, P. *Phys. Rev. Lett.* **1996**, *77*, 1536−1539.
(17) Jacobs, K.; Seemann, R.; Schatz, G.; Herminghaus, S. *Langmuir* **1998**, *14*, 4961−4963.
(18) Jacobs, K.; Herminghaus, S.; Mecke, R. *Langmuir* **1998**, *14*, 965−969.
(19) Sheiko, S.; Lermann, E.; Möller, M. *Langmuir* **1996**, *12*, 4015−4024.
(20) Dedecker, K.; Groeninckx, G. *Pure Appl. Chem.* **1998**, *70*, 1289−1293.
(21) Dedecker, K.; Groeninckx, G. *Polymer* **1998**, *39*, 4985−4992.
(22) Dedecker, K.; Groeninckx, G. *Polymer* **1998**, *39*, 4993−5000.
(23) Dedecker, K.; Groeninckx, G. *Polymer* **1998**, *39*, 5001−5010.
(24) Schubert, D. W. *Polym. Bull.* **1997**, *38*, 177−184.
(25) Biegen, J. F.; Smythe, R. A. *Proc. SPIE, Int. Soc. Opt. Eng.* **1988**, *897*, 207−217.

(26) Sung, L.; Karim, A.; Douglas, J. F.; Han, C. C. *Phys. Rev. Lett.* **1996**, *76*, 4368−4371.
(27) Hashimoto, T.; Takenaka, M.; Jinnai, H. *J. Appl. Crystallogr.* **1991**, *24*, 457−466.
(28) Fukao, K.; Miyamoto, Y. *Phys. Rev. E* **2000**, *61*, 1743−1754.
(29) Forrest, J. A.; Dalnoki-Veress, K.; Dutcher, J. R. *Phys. Rev. E* **1997**, *56*, 5705−5716.
(30) Joly, S.; Raquois, A.; Paris, F.; Hamdoun, B.; Auvray, L.; Ausserre, D.; Gallot, Y. *Phys. Rev. Lett.* **1996**, *77*, 4394−4397.
(31) Reiter, G. *Europhys. Lett.* **1993**, *23*, 579−584.
(32) Müller-Buschbaum, P.; Gutmann, J. S.; Stamm, M. *Phys. Chem. Chem. Phys.* **1999**, *1*, 3857−3863.
(33) Müller-Buschbaum, P.; Gutmann, J. S.; Stamm, M.; Cubitt, R.; Cunis, S.; von Krosigk, G.; Gehrke, R.; Petry, W. *Physica B* **2000**, *283*, 53−60.
(34) Kim, J. H.; Barlow, J. W.; Paul, D. W. *J. Polym. Sci., Part B: Polym. Phys.* **1989**, *27*, 223.
(35) Scott, C.; Macosko, C. *J. Polym. Sci., Part B: Polym. Phys.* **1994**, *32*, 205−213.
(36) Cho, K.; Seo, K. H.; Ahn, T. O.; Kim, J.; Kim, K. U. *Polymer* **1997**, *38*, 4825−4830.

MA000287K